Physics of Fluids

Laser induced fluorescence studies on the distribution of surfactants during drop/interface coalescence

Cite as: Phys. Fluids **31**, 012106 (2019); https://doi.org/10.1063/1.5059554
Submitted: 20 September 2018 . Accepted: 04 December 2018 . Published Online: 08 January 2019

Teng Dong, Weheliye Hashi Weheliye, and Panagiota Angeli

Physics of Fluids ARTICLE scitation.org/journal/phf

Laser induced fluorescence studies on the distribution of surfactants during drop/interface coalescence

Cite as: Phys. Fluids 31, 012106 (2019); doi: 10.1063/1.5059554
Submitted: 20 September 2018 • Accepted: 4 December 2018 •
Published Online: 8 January 2019

Teng Dong, Weheliye Hashi Weheliye, and Panagiota Angeli[a]

AFFILIATIONS

ThAMeS Multiphase, Department of Chemical Engineering, University College London, London WC1E 7JE, United Kingdom

[a]Author to whom correspondence should be addressed: p.angeli@ucl.ac.uk

ABSTRACT

The spatiotemporal distribution of fluorescent surfactants on the merging interfaces during the coalescence of an aqueous drop with an organic/aqueous flat interface was studied experimentally with high-speed laser induced fluorescence. The aqueous phase was a 46% glycerol solution, while the organic phase was a 5 cSt silicone oil. A fluorescently tagged surfactant was used at a concentration of 0.001 mol/m^3 in the aqueous phase. To vary the concentration of surfactants on the interfaces, the drop and the flat interface were left to stand for different times before the coalescence experiments (different interface ages). It was found that when a drop rested on the interface, the surfactants adsorbed on the interfaces were swept outwards by the draining liquid film between the drop and the flat interface and reached a peak value at $0.75R_h$ away from the centre of the film, where R_h is the horizontal drop radius. After the film rupture, the concentration of the surfactants at the tip of the meniscus increased. Once the film had retracted, the concentration of the surfactants peaked at the meniscus at the bottom of the drop. As the liquid in the drop started to merge with its homophase, the drop formed a cylinder from the upward capillary waves on the drop surface. The surfactant concentration was found to be low at the top of the liquid cylinder as the interface was stretched by the convergence of the capillary waves. Subsequently, the cylinder began to shrink and the top part of the drop acquired a high surfactant concentration.

I. INTRODUCTION

The phenomenon of drop coalescence is often encountered in emulsions and dispersions in many industrial fields, including oil production and processing,[1–3] milk production,[4] drug encapsulation,[5,6] and liquid jet atomization.[7,8] The rate of drop coalescence plays a key role in controlling the stability of emulsions. Generally, surfactants either naturally exist or are artificially introduced to these liquid systems to change the stability by modifying the coalescence rate. Previous studies have shown that surfactants affect the whole coalescence process from the drop rest at the early stages to the subsequent merging process of either drops or drops with interfaces. The drop rest time refers to the time required for the thinning of the trapped film between the drop and the bulk liquid homophase from its initial thickness to the final critical thickness where rupture occurs. In drop coalescence with a liquid-liquid interface, many scientists experimentally observed that the rest times increased considerably when surfactants were present.[9–12] The drop rest times can vary significantly even under the same experimental conditions, and this behaviour is more pronounced in the presence of surfactants. Hodgson and Woods[13] suggested that the surfactants altered the draining behaviour of the thin film. In their experiments, the thinning of the film was found to be relatively symmetrical in the absence of surfactants, while a dimpled film, with a thicker part at the centre and a thinner barrier ring at the circumference, commonly occurred when surfactants were present. Many researchers suggested that the dimple was created by Marangoni backflow in the trapped film.[14–18] When the liquid

in the film is squeezed outwards, the surfactants on the interface are swept to the border and finally accumulate at the barrier ring, resulting in a higher surfactant concentration in that region. The non-uniform distribution of surfactants leads to the variation of surface tension along the interface. Marangoni stresses develop which oppose the outward liquid flow and create a backflow in the film that thickens its central part. Considering Marangoni forces, the drainage of the thin film in drop-drop binary coalescence with surfactants was numerically analyzed,[19,20] and the results were in good agreement with previous experiments.[21] By contrast, other studies supported that the Marangoni backflow was not strong enough to suppress the outward flow in the film[22,23] and the only role of the Marangoni stresses was to suppress the inner circulation in the drops and make the interface rigid. Giribabu and Ghosh[23] further derived a stochastic model to estimate the drop rest times based on the uneven distribution of surfactants along the interface, and the results were consistent with previous experimental data. Even though there is disagreement on how surfactants affect the film drainage, the uneven distribution of the surfactants on the interface is generally accepted by most researchers.

Rupture occurs when the attractive van der Waals forces are large enough to overcome the repulsive forces at a critical thickness of the film. Afterwards, the neck connecting the drop with the bulk liquid or the other drop starts to expand driven by the capillary forces at the highly curved meniscus. A full understanding of the neck expansion process is of great importance to applications where coalescence affects the drop size, such as drug capsulation,[24] nanoparticle synthesis,[25] and intensified liquid extractions.[26] Based on whether the inertial or the viscous force mainly resists the capillary force, two regimes are generally identified. At the beginning when the meniscus size is small, the increase in the neck radius against rupture time follows a linear relationship. The viscous force dominates the process, defining the viscous regime, which is characterized by the time scale $t_{viscous} = R\mu/\sigma$. Here, R is the drop radius, μ is the viscosity of the drop liquid, and σ denotes the interfacial tension. When the neck is sufficiently large, the inertial force mainly controls expansion (inertial regime) which is characterized by the time scale $t_{inertial} = (\rho R^3/\sigma)^{1/2}$, where ρ is the density of the drop liquid.[27–31] Chinaud, Voulgaropoulos, and Angeli[31] investigated the neck growth in drop/interface coalescence under various surfactant concentrations. The results showed that the neck radius increased linearly in the viscous regime for both the pure and the surfactant systems. The authors showed that the curves in all systems collapsed to a single line when the local surfactant concentration at the meniscus was taken as twice the surfactant concentration in the bulk. Martin and Blanchette[32] from numerical simulations showed that the surfactant concentration at the neck could be four times higher than that in the rest of the film, which has not yet been confirmed by any experimental results. The coalescence of a surfactant-laden drop with a surfactant-free drop was also studied recently.[33–35] The neck on the side of the surfactant-free drop was found to expand faster than on the other side, which confirmed the results by Blanchette, Messio, and Bush[36] that the interface with high surface tension tends to pull the low surface tension area to create a tangential flow along the interface.

Apart from their effect on drop rest and neck growth, surfactants also have a significant impact on the subsequent merging of the liquids. Weheliye, Dong, and Angeli[37] found that the drop shape changed significantly when surfactants were present during coalescence. They found that for a drop coalescing with a flat interface in a surfactant-free system, the drop summit could reach a minimum height far below the initial interface position and rebound in a short time. When surfactants were present, the drop summit approached the final flat interface slowly. In addition, the vortices generated at the onset of the meniscus rupture were inhibited by surfactants as well. Surfactants also affect the appearance of partial coalescence. The partial coalescence region in an Oh-Bo based map is largely reduced when surfactants are present, and the size of the daughter drops in the inertial-capillary regime is also reduced.[38,39] Martin and Blanchette[32] showed from numerical studies that the uneven distribution of surfactants along the drop surface generated tangential stresses which helped the daughter drops to reduce in size and could prevent partial coalescence.

All stages of the coalescence phenomenon are influenced by the uneven distribution of surfactants on the interface. However, it is still challenging to directly measure the surfactant concentration along the evolving drop surface. In most of the existing studies, the distribution of the surfactants has been estimated indirectly. According to the Szyszkowski-Langmuir equation as shown in Eq. (1), the surfactant concentration at the interface can be estimated if the data of the interfacial tension is acquired,[23,40,41]

$$\sigma = \sigma_0 - RT\Gamma_\infty \ln(1 + K_L\varphi), \tag{1}$$

where σ_0 is the interfacial tension for the system without surfactant, R is the universal gas constant, T is the temperature, Γ_∞ is the surfactant concentration at the saturated interface, φ is the surfactant concentration in the bulk liquids, and K_L is the equilibrium constant, which indicates the ratio of the rates of surfactant adsorption and desorption. Once the equilibrium interfacial tensions under various surfactant concentrations in the bulk are known, the values of Γ_∞ and K_L can be calculated by fitting the data. Then the surface excess related to each bulk concentration can be calculated through the Langmuir isotherm,

$$\Gamma = \Gamma_\infty K_L\varphi/(1 + K_L\varphi). \tag{2}$$

The model can estimate the surface excess of the surfactant but cannot indicate the local distribution of the surfactants along the drop surface. Recently, an advanced technique, Spatiotemporal Filter Velocimetry (SPV), was applied by Hosokawa *et al.*[42] to measure the local Marangoni stresses on the drop surface, based on the velocity gradients at the vicinity of the surface. The local surfactant concentration

was subsequently estimated using Frumkin's equation. The SPV method is also indirect and needs very fine spatial resolution, which increases the complexity of the experiments. Planar Laser Induced Fluorescent (PLIF) has also been used in many studies, where a fluorescent surfactant is spread on a thin liquid layer, and the concentration is related to the intensity of the emitted light when illuminated by a laser.[43–46] This technique has so far only been used to investigate the spreading of surfactants along a liquid/air surface.

The review above reveals that there is limited work on the dynamics of coalescence of a drop with another homophase (drop or bulk liquid) in the presence of surfactants. The available experimental studies mainly focus on the evolution of the interfaces but do not consider the surfactant distribution which is very challenging to obtain experimentally. On the other hand, the limited numerical studies available on the surfactant distribution have not been validated experimentally. From these studies, a number of hypotheses have been proposed such as (1) surfactants can accumulate at the film barrier ring area during drop rest;[19,20,23] (2) the surfactant concentration at the meniscus tip is higher than that of the rest of the film during the retraction;[31,32] (3) the distribution of surfactants along the drop surface as the drop merges with the homophase is uneven.[32] The aim of this paper is to experimentally address questions related to the spatial distribution of surfactants at the interfaces during coalescence. A novel experimental technique, high speed planar laser induced fluorescence, combined with a fluorescent surfactant is used to study the coalescence of a drop with a liquid-liquid interface. Varying initial surfactant concentrations at the interfaces were achieved by allowing the drop and the flat interface to stand for different times before the coalescence experiments. The distribution of surfactants was studied during the three stages of coalescence, namely, film thinning, meniscus rupture, and final drop merging with the homophase.

II. EXPERIMENTAL SETUP AND METHODOLOGY

A. Experimental apparatus and materials

The schematic of the Planar Laser Induced Fluorescent (PLIF) experimental setup is shown in Fig. 1. The system consists of a rectangular vessel made from acrylic with 5 cm × 5 cm bottom width and 15 cm height. The aqueous phase was placed at the bottom, and the organic phase was added on the top forming an interface in the middle of the vessel. A drop of the same liquid as the aqueous phase was created within the organic phase through a flat-ended nozzle (inner diameter ID = 2 mm) at around 1 cm above the interface to avoid any oscillations as the drop falls towards the interface. The other side of the nozzle was connected to a syringe which was mounted on a programme-controlled Aladdin® syringe pump. The flow rate was set at 0.2 ml/min for a better control of the drop sizes, which were 5.90 ± 0.14 mm in horizontal diameter for all the experimental conditions. The sizes were measured when the drops rested on the interface.

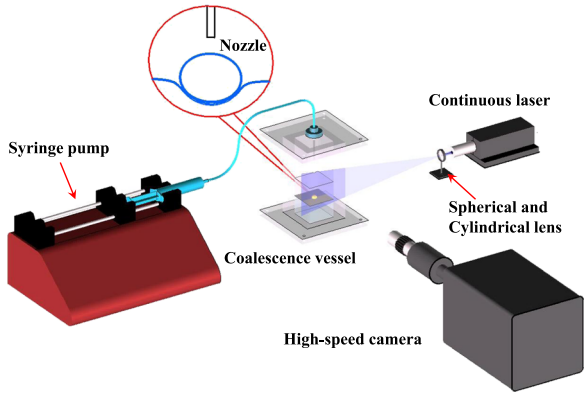

FIG. 1. Schematic of the PLIF experimental setup.

The organic phase was a 5 cSt silicone oil (density ρ_s = 914 kg/m^3, viscosity μ_s = 4.57 mPa s), and the aqueous phase was a water-glycerol mixture for all the tests. The volume concentration of the glycerol in the aqueous phase was set at 46% to match the refractive index of the oil (r = 1.3925 at 25 °C) and avoid any light distortions at the interface when the laser illumination was used. The refractive index was measured by using an Abbe5® refractometer. The density and viscosity of the 46% glycerol solution were ρ_d = 1150 kg/m^3 and μ_d = 4.35 mPa s, respectively.

For the experiments, a fluorescently tagged surfactant NBD-PC (1-palmitoyl-2-12-[(7-nitro-2-1,3-benzoxadiazol-4-yl) amino] lauroyl-sn-glycero-3-phosphocholine) with molecular weight equal to M = 856.038 g/mol was dissolved in the aqueous phase. The surfactant absorbs at 464 nm and emits at 531 nm. Ultrasound was used to ensure homogeneous mixing of the surfactant in the aqueous phase. The dynamic interfacial tensions of the interfaces at the equilibrium level between the 5 cSt silicone oil and the aqueous solutions with various concentrations of NBD-PC were measured with the Du Noüy ring method (Kruss® surface tension meter). The interfacial tensions under the same surfactant concentration were reproducible with a relative standard deviation less than 5%. The equilibrium interfacial tension is presented in Fig. 2 for different surfactant concentrations in the aqueous phase. As can be seen, NBD-PC is able to lower the interfacial tension by around 0.020 N/m from φ = 0 mol/m^3 to the critical micelle concentration, which is reached at a surfactant concentration $\varphi \approx 0.013$ mol/m.[3] For the coalescence experiments, the concentration of the surfactant in the aqueous solution was set at 0.001 mol/m,[3] which is significantly lower than the critical micelle concentration. This concentration was selected because it lowers sufficiently the interfacial tension, has adequate fluorescence for the PLIF experiments, while it prevents the formation of surfactant micelles in the aqueous phase that can interfere with the PLIF experiments.

In the coalescence experiments, the distribution of the surfactants for the processes from the drop resting on the

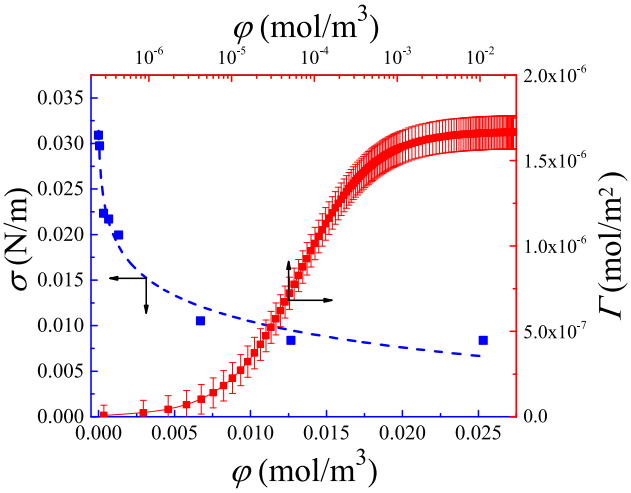

FIG. 2. The interfacial tension of the interface between the 5 cSt silicone oil and the 46% glycerol solution against the concentration of the NBD-PC. The squares indicate the interfacial tension under various surfactant concentrations. The data were plotted against the bottom linear scale of φ. The dashed line is fitted to the experimental data. The continuous line is the prediction of the surfactant excess on the interface based on the Langmuir adsorption model. The data were plotted against the top log scale of φ.

interface, the film thinning and rupture, and the merging of the drop with the bulk homophase were investigated with high-speed planar laser induced fluorescence technology. As shown in Fig. 1, the centre plane of the drop was illuminated by a laser sheet. The light was generated by using a Laserglow5® continuous laser (473 nm, 300 mW), which was connected to a spherical and a cylindrical lens in series to create a 1 mm laser sheet. The laser along with the optical lenses was mounted on a mobile stage and adjusted to bisect the centre plane of the drop. In all experiments, the output power of the laser was kept constant to prevent any energy deviations. For better visualization and consistent comparisons, only the coalescence events where the rupture points are on the laser plane were considered. A Phantom high speed camera, equipped with a mono-zoom Nikon lens, which gave a spatial resolution of 13 μm/pixel, was placed perpendicular to the laser sheet to capture the process of coalescence. A green filter was connected to the lens to eliminate reflections. To capture the very fast film rupture and the liquid merging steps, the camera was operated at a high frame rate of 2000 fps. The whole setup was mounted on an optical table, and the relative spatial locations among the high-speed camera, the continuous laser, and the coalescence vessel were fixed to avoid any mismatch between runs. During each experiment, the temperature was kept constant in the lab. As the drops were generated in the organic phase and the whole coalescence process occurred within the liquid system, the effect of the environmental humidity was considered negligible.

B. Experimental methods

As pointed out by Eastoe and Dalton,[47] the adsorption of the surfactant molecules from the bulk liquids to the interface is a dynamic and slow process. For the surfactant used in this work, it takes hours for the interfacial tension to reach the final equilibrium value. To account for this, the coalescence experiments were carried out for different ages of the drop surface and the interface. Here, the drop surface (or the interface) age T refers to the time from when the drop contacts the surrounding organic phase (or the organic phase contacts the bulk aqueous phase) to the time when the coalescence experiment starts. Drop surface ages from T = 0 min to T = 900 min were studied. In the fresh system (T = 0 min), the interface was generated by adding the liquids in the vessel, while the drop was formed in the oil and immediately after it was deposited on the interface. For the experiments carried out at different ages, the drop was generated within and was kept attached to the nozzle for the required age T, before it was released to approach the interface to start the coalescence process. The initial sizes of the pending drops for all the tests were kept constant by the syringe pump. Since the drop surface age and the interface age are equal in the experiments, the surface age T will be used in the rest of the paper to represent the ages of the two. Typical fluorescent images of drops resting on the interface for various drop surface ages are shown in Fig. 3. As can be seen, for T = 0 min, the drop surface has similar brightness as the rest of the liquid inside the drop. The part at the bottom of the drop appears brighter because it is the location where both interfaces, the drop and the liquid-liquid one, meet. At longer ages, the brightness of the drop surface is higher than inside the drop, which indicates that the surfactant is adsorbing to the drop surface.

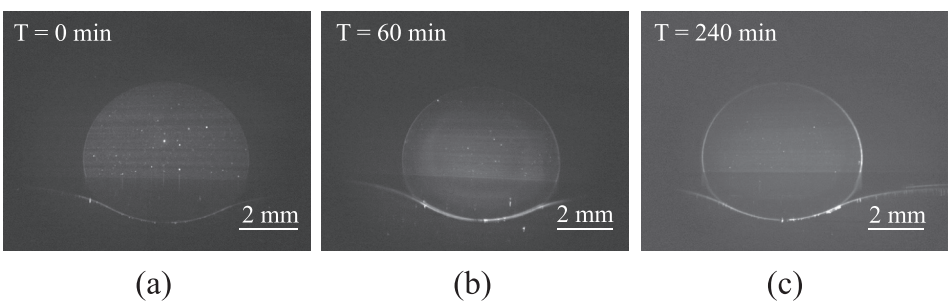

FIG. 3. Raw fluorescent images of a drop resting on the interface for (a) T = 0 min, (b) T = 60 min, and (c) T = 240 min.

C. Fluorescent imaging and calibration

In the PLIF measurements, the concentration of the surfactants is estimated by detecting the fluorescence intensity in the recorded images. To generate the calibration curve, various concentrations of NBD-PC from 0 to 0.0078 mol/m^3 were dissolved in the bulk 46% glycerol solution and the corresponding intensity was measured. For each concentration, more than 200 images were captured to produce the average fluorescent intensity. To avoid the effect of the adsorption of surfactants on the surface on the calibration results, the bulk liquid at each concentration was mixed well and measurements were taken immediately after. To account for any changes in the fluorescence intensity because of the chemical stability of the surfactant, the calibration was repeated three times with a 24 h difference between each test. Between experiments, the liquids were stored in a dark environment to prevent photo-dissociation.

The fluorescence intensity as a function of the surfactant concentration is shown in Fig. 4. As can be seen, the fluorescence intensity increases exponentially with the surfactant concentration in the range of the measurements. By fitting the data, the following correlation was found that links the fluorescence intensity, I, to the corresponding surfactant concentration:

$$\varphi = I^{2.27}. \tag{3}$$

From the volume concentration φ, the surface concentration, Γ, was calculated, which is generally used to describe the surface excess of surfactants.[20,22,43,44] For an interface with given thickness, the surface excess can be obtained by integrating the volume concentration φ along the surface thickness h, which could be regarded as constant.[12]

The theoretical surface excess of the NBD-PC on the interface between the 5 cSt silicone oil and the 46% glycerol solution was also calculated to validate the calibration results. According to the Langmuir isotherm [Eq. (2)], the surface excess of the surfactant on an interface can be calculated if the two parameters Γ_∞ and K_L are known. By fitting the measured interfacial tension points at various surfactant concentrations (dashed line shown in Fig. 2), it was found that $\Gamma_\infty = 1.67 \times 10^{-6}$ mol/m^2 and $K_L = 15\,249$ m^3/mol. When these values are substituted into Eq. (2), the surface excess corresponding to the bulk surfactant concentration can be calculated, as shown in Fig. 2 by the continuous (red) line. For the applied surfactant NBD-PC, the surface excess at the flat liquid/liquid interface is in the order of $\Gamma = 0$–1.67×10^{-6} mol/m^2 depending on the age of the interface. The surface concentration Γ obtained through the calibration curve, from Eq. (3), using the average intensity at the interface was in reasonable agreement with the values estimated from the Langmuir adsorption model. However, deviations could not be avoided as the calibration was not directly based on the intensity from the interface. As reported by Fallest *et al.*,[43] a similar fluorescent surfactant, NBD-PC, was employed on a thin liquid layer, and the concentrations measured at the interface were found to be linear with the intensity of the emitted light. Therefore, for the rest of this study, a linear relationship is assumed between the surface concentration and the fluorescent intensities emitted at the interface. The surface concentration Γ was normalized with the maximum surfactant concentration at the drop surface at T = 900 min, i.e., $\Gamma^* = \Gamma/\Gamma^{900}_{max}$. The normalized surfactant concentration Γ^* along the drop surface was extracted for different surface ages T. As shown in Fig. 5, with the drop surface aging, the surfactant concentration Γ^* was increased.

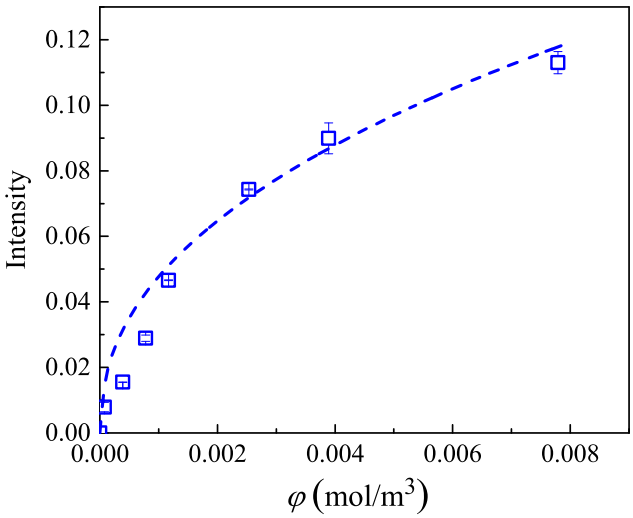

FIG. 4. Calibration of surfactant fluorescence intensity as a function of the surfactant concentration. The squares represent the averaged fluorescence intensity at each concentration, and the dashed line shows the fitting trend.

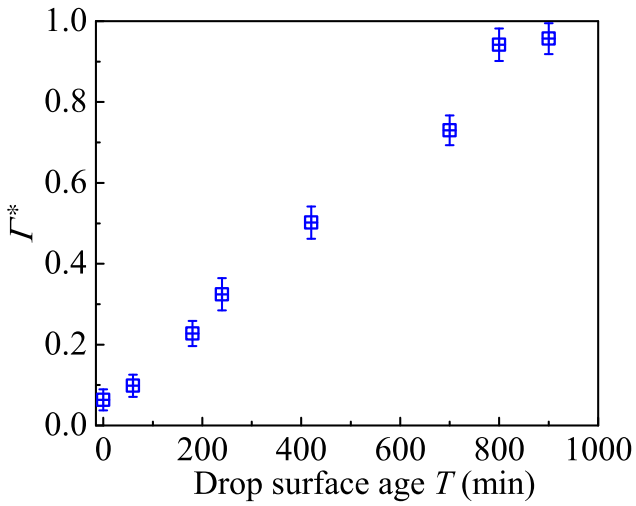

FIG. 5. The average of the normalized surfactant concentration Γ^* along the drop surface for different surface ages T. Here, the normalization of concentration $\Gamma^* = \Gamma/\Gamma^{900}_{max}$. The error bars show the variation of Γ^* along the drop surface.

D. Image processing and challenges

In this section, a detailed analysis of the image processing methodology and the challenges encountered will be outlined. First, it is necessary to properly detect the interface region for the subsequent calculations of the surfactant concentration. This is shown below for the interface at the bottom of the drop as a representative example. Initially the intensities along vertical lines in the image [e.g., L1, L2, and L3 in Fig. 6(a)] are plotted, as shown in Fig. 6(b). When the interface region is crossed, the intensity increases sharply. The location of the peak point was then defined as a y value. Intensities were recorded every 5 vertical columns, and the data were smoothed by cubic smoothing spline functions to produce a continuous curve.

The thickness of the interface was then calculated by measuring the bandwidth of the sharp increase in the intensity curve, as shown in Fig. 6(b), between the dashed lines. This interface thickness was thin (0.026 mm) for the drop surface at T = 0 min, while it was able to reach around 0.1 mm for T = 900 min. The variation was about 0.06 ± 0.035 mm for all the tests.

However, it should be noted that the thickness of the interface shown in the images can be much larger than the thickness of the real interface[48] because of the curvature of the drop surface and the light diffraction. The effect of the curvature of the drop surface can be eliminated by generating drops with a diameter much larger than the laser sheet thickness. In this work, the thickness of the laser sheet was 1 mm and the monozoom Nikon lens connected to the camera gave a depth of field (DOF) approximately equal to 0.5 mm. The effect of the curvature of the drop surface could become significant when the drop diameter was close to 1 mm. In the current study, the drops were about 6 mm in diameter.

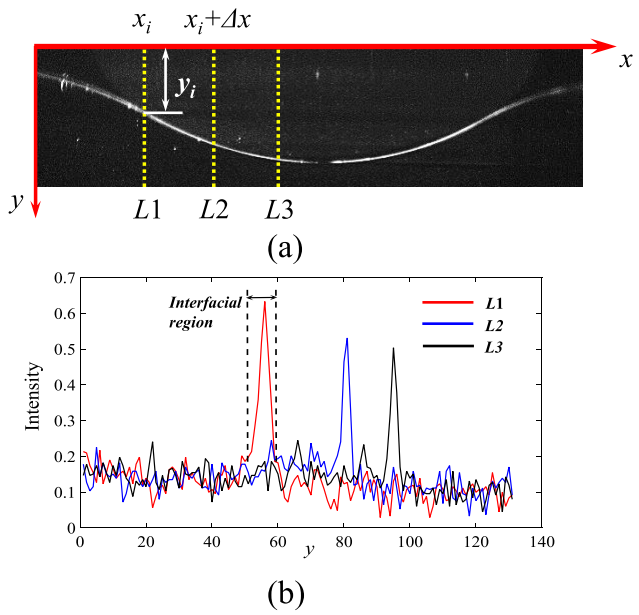

FIG. 6. (a) Schematic of the interfacial region detection and (b) intensity curves along the lines *L*1, *L*2, and *L*3.

Light diffraction can also affect the calculation of the interface thickness. To estimate this, the averaged surfactant concentrations were calculated from two different approaches. The first approach was to calculate the average surfactant concentration Γ_1 considering the maximum value and the values at 2 neighbouring points, while the second approach was to average the surfactant concentration Γ_2 among all the values in the interfacial region [within the dashed lines in Fig. 6(b)]. It was found that for the drop surface, the averaged surfactant concentration $\Gamma_1 = (1.1 \pm 0.04)\Gamma_2$ depending on the interface aging time. For the interface region that combines the drop surface and the phase interface, $\Gamma_1 = (1.2 \pm 0.052)\Gamma_2$. It appears that the interfacial thickness does not significantly affect the results. The first approach was used below to calculate the surfactant concentration at the interface at different aging times.

III. RESULTS AND DISCUSSION

A. Drop rest phenomenon

Previous studies have shown that Marangoni stresses resulting from the uneven distribution of the surfactants along the interface largely affect the film drainage process.[20,22,49] However, this phenomenon has not been observed experimentally previously. In this section, the surfactant concentration Γ^* along the interface where the drop surface contacts the liquid-liquid interface is investigated for various surface ages T.

Figure 7 shows the normalized surfactant concentration Γ^* along the interface where the drop contacts the bulk phase for different surface ages. The surfactant concentration Γ^* was averaged over 5 tests for the fresh system with T = 0 min.

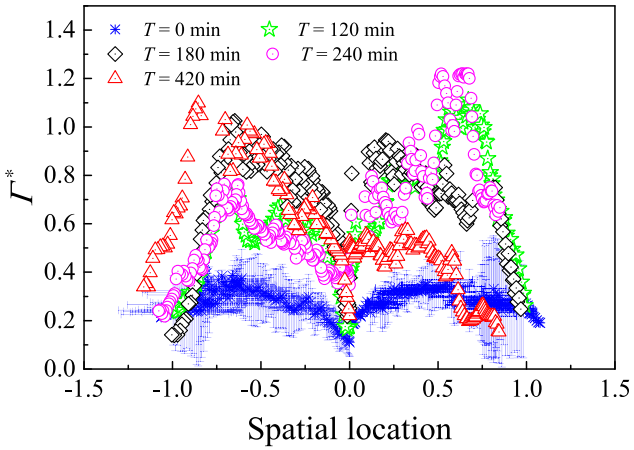

FIG. 7. Surface concentration of surfactants Γ^* along the interface. The distance, indicating the arc-length from the centre, is normalized by the horizontal drop radius R_h. The negative values of the distance indicate the area on the left, and the positive values indicate the area on the right from the centre.

For consistency, all measurements were taken at the last time step just before the onset of the film rupture. When the surface is aged to T > 60 min, the drop rest times are long and in some cases can exceed the sampling time of the high-speed camera. Therefore, the results shown for large T are from single representative tests since it was difficult to capture and repeat exactly the coalescence events. As the thickness of the trapped film between the drop and the bulk liquid is less than a micrometer at the final moments just before film rupture,[50,51] it is not possible to distinguish the drop surface from the phase interface. Thus the combined surfactant concentrations from both the drop surface and the interface were evaluated and plotted.

For the fresh system at T = 0 min, the surfactants have little time to adsorb to the interface, and the surface concentration along the interface is much lower than the saturated concentration, as shown in Fig. 7. During the draining process, the surfactants at the interface are driven outwards by the film liquid. As a result, the surface concentration Γ^* is low at the centre and gradually increases towards the outside until a maximum value is reached at around $0.7–0.75R_h$, where R_h refers to the horizontal drop radius. The area with the highest surfactant concentration is generally considered to be at the barrier ring, where the film is at its thinnest.[12,20,22,23,52] Hodgson and Woods[13] reported that the barrier ring diameter is expanding during the drainage process. In the current experiments where both the drop and the interface are deformable, the radius of the barrier ring, R_b, just before rupture can be estimated from the work of Princen,[53]

$$R_b = 2R_d^2\sqrt{\frac{\Delta\rho g}{3\sigma}}. \tag{4}$$

According to Eq. (4), the radius of the barrier ring for a 5.9 mm drop is around $0.68R_h$. From Fig. 7, the radius of the circumference where surfactants accumulate is around $0.7R_h$. Thus the radius of the location of the maximum surfactant concentration is found to be close to the barrier ring.

As the surface age T increases, there is more time for the surfactant to adsorb to the interface. The film drainage time also increases after the drop contacts the interface,[23] and more time is allowed for the fluid in the film to sweep the surfactant molecules toward the barrier ring area. The related maximum surfactant concentration resulting from the accumulation can reach to around $1\Gamma_{max}^{900} – 1.2\Gamma_{max}^{900}$ for T > 120 min, which is much larger than that of the centre area. The increase in the surfactant concentration from the centre toward the barrier area is in good agreement with the theoretical estimations by Burrill and Woods.[54] Interestingly, the maximum surfactant concentration stays at about $1\Gamma_{max}^{900} – 1.2\Gamma_{max}^{900}$ and does not increase with the surface age. This is attributed to Marangoni flows. As more surfactants are concentrated on the interface, more molecules are swept outwards during the film drainage; the increased surfactant concentration gradient along the interface can create significant Marangoni surface flows that resist further outward movement of the surfactants. A dynamic balance between the film flow and the Marangoni backflow is established that keeps the surfactant distribution constant.

The distribution of the surfactants is relatively symmetrical on both sides of the interface for T = 0 min, as shown in Fig. 7. However, at larger surface ages, the distribution is not symmetrical anymore. The asymmetry is reflected in both the concentration of the surfactant along the interface and the location of the area with the highest concentration. For T = 120 min and 240 min, a distinct peak of the surfactant concentration is observed at $0.75R_h$ away from the centre on the right, while the interface on the left has a lower surfactant concentration. For T = 420 min, the opposite is observed. For T = 180 min, the peak value of the surfactant concentration is closer to the centre on the right than on the left side. The non-symmetrical distribution of surfactants along the contact interface is mainly attributed to the variations from the irregular draining of the thin film. As discussed by Chan, Klaseboer, and Manica,[55] the film thinning is affected by a number of factors including the initial separation between the drop and the interface, the approaching manner of the drop, the film viscosity, the interface mobility, and the surface tension. Different types of thinning behaviour were observed accordingly,[13,54,56] including symmetrical draining, left side faster draining, and right side faster draining.

At the early stages of coalescence just after the drop has contacted the interface, a dimple appears in the film, which drains out subsequently to bring the drop surface close to the interface leading finally to rupture.[55,57–59] The structures of the thin film at the initial stages of the drop rest for different surface ages are shown in Fig. 8. For most tests with the fresh

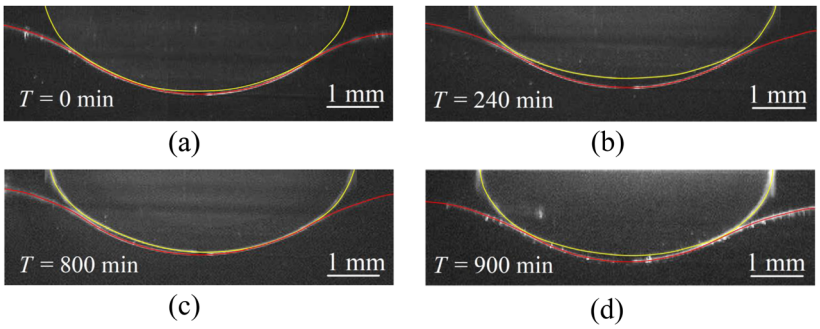

FIG. 8. Typical structures of the thin film trapped between the drop and the bulk liquid at the initial stages of the rest phenomena for varying surface ages. The drop surface and the phase interface are highlighted with yellow and red lines, respectively, to help visualization.

system of T = 0 min, the thickness of the thin film is small and the dimple structure is not obvious. For some cases at T = 240 min and T = 900 min, a dimple-shaped film with a thinner part at the barrier ring and a thicker part at the centre is observed. As was mentioned before, non-symmetrical dimpled films can appear as well, as shown in Fig. 8(c) for T = 800 min. As more surfactants are accumulated at the circumference at long surface age T, it has been suggested that the dimple is created by the strong Marangoni backflow which suppresses the outward lubrication flow.[15–17,20] Ghosh and Juvekar,[22] however, considered that the Marangoni flow decreases only the mobility of the drop surface and is too weak to resist the lubrication flow that drains the film. This explanation seems to agree better with the experimental results here which showed that the film drainage was still fast even for T = 800 min when a significant surfactant concentration gradient along the interface exists.

The film drainage patterns seem to affect the distribution of the surfactants shown in Fig. 7. For T = 0 min, where the film drains symmetrically, the distribution of surfactants is also symmetrical. As the trapped film and the dimple structure become thicker at large age drop surfaces, the liquid drainage time is increased and loses its symmetry [Figs. 8(b)–8(d)]. This will affect the distribution of the surfactants as well and may give rise to instabilities. As a result, it is more likely to observe the non-symmetrical distribution of surfactants for longer age drops.

B. Neck-growth

When the film rupture occurs, the meniscus (or neck) which links the drop and the bulk phase grows rapidly. It should be noted that in all cases reported here, the rupture points occurred in the laser plane. It was observed from the images that the drop surface folded up if the rupture points occurred out of the view plane. As it was found in previous studies, the rupture locations could be affected by the surfactant concentration.[37,39] When the surfactant concentration in the bulk is increased close to the critical micelle concentration, the interface can be largely deformed and the rupture points are shifted further away from the centre point. However, as the surfactant concentration in the bulk used here was 0.001 mol/m^3, which was far less than the critical micelle concentration, the location of the rupture points was not significantly affected. Also the aging times had negligible effect on the location of the rupture point in this study. Numerically it has been found that the meniscus at the initial stages of retraction has a bulge structure.[27,60] As the tip is accelerated by the huge local curvature of the meniscus, its velocity is much higher than that of the liquid in the film which is gradually collected in the growing toroidal body. The findings have been confirmed by many experimental observations in the absence of surfactants.[61–63]

The local structure of the meniscus tip and the surfactant concentration in this region are shown in Fig. 9 for different surface ages. The coalescence time t in the figure refers to the time after the rupture of the thin film. Due to the instability of the expanding rim, a series of tendrils are created and detached from the rim to form tiny drops,[62] shown as bright spots in the images. The bright bulge at the edges of the meniscus cannot be seen for all the surface ages in the viscous regime from t = 1 ms to t = 2 ms because of two main reasons. First, the radius of the initial bulge r_b is theoretically in the order of $r_m^{3/2}$, where r_m is the radius of the neck.[27] At the viscous regime, the neck radius r_m is very small, and the related bulge cannot be seen accordingly. Second, the interfacial tension is largely reduced when surfactants are present and the meniscus retracts at a lower speed than in the surfactant-free system. When the neck growth advances in the inertial regime from t = 4 ms to t = 9 ms, the bulge size increases in varying degrees for different surface age T. For T = 0 min, the bulge is small, while it becomes larger when the drop surface has aged to T = 240 min and 300 min, as shown in Fig. 9. For an aged surface with large T, dimple structures form at the film; a large amount of the fluids is collected there which increases the size of the bulge as the meniscus advances through this thick part of the film.

The distribution of the surfactant concentration along the interface for the surface age of T = 0 min is shown in Fig. 10 as a representative example. Only the left tip which travels over a longer distance is plotted. When the film rupture happens, the rapid retraction of the tip reduces the interfacial area. In addition, there is not enough time for the surfactants to diffuse or desorb from the interface. Thus the surfactants are accumulated at the tip and increase the local concentration.

To quantitatively investigate the accumulation of the surfactants at the neck tip, the space averaged surfactant concentration Γ^*_{tip} at the tip area is calculated according to Eq. (5),

$$\Gamma^*_{tip} = \frac{\int \Gamma^* d\mathrm{A}}{\mathrm{A}_{tip}}. \tag{5}$$

The area of the tip A_{tip} is found from subtraction of two consecutive images. For consistency, only the side of the neck that travels longer is considered for all the cases. The evolution of the surfactant concentration at the tip area is plotted in Fig. 11 for different surfactant ages. The data are averaged over 5 tests for surface ages T = 0 min and 60 min, while for T = 240 min and 420 min, only representative data are plotted from one test. The accuracy in determining the onset of the rupture is 0.5 ms for all the tests as the frame rate of the high-speed camera is 2000 fps.

For T = 0 min, the increase in the tip concentration is small compared to the other three cases, which is mainly due to the few surfactant molecules present at the interface. As Fig. 7 shows, the initial surfactant concentration at the phase interface is much lower for T = 0 min than for the other cases. The retraction of the tip in this case does not accumulate enough surfactant molecules. In addition, the neck tip moves faster for T = 0 min than for the other ages (see Fig. 12), and the area A_{tip} is relatively larger. For T = 60 min, a large increase in

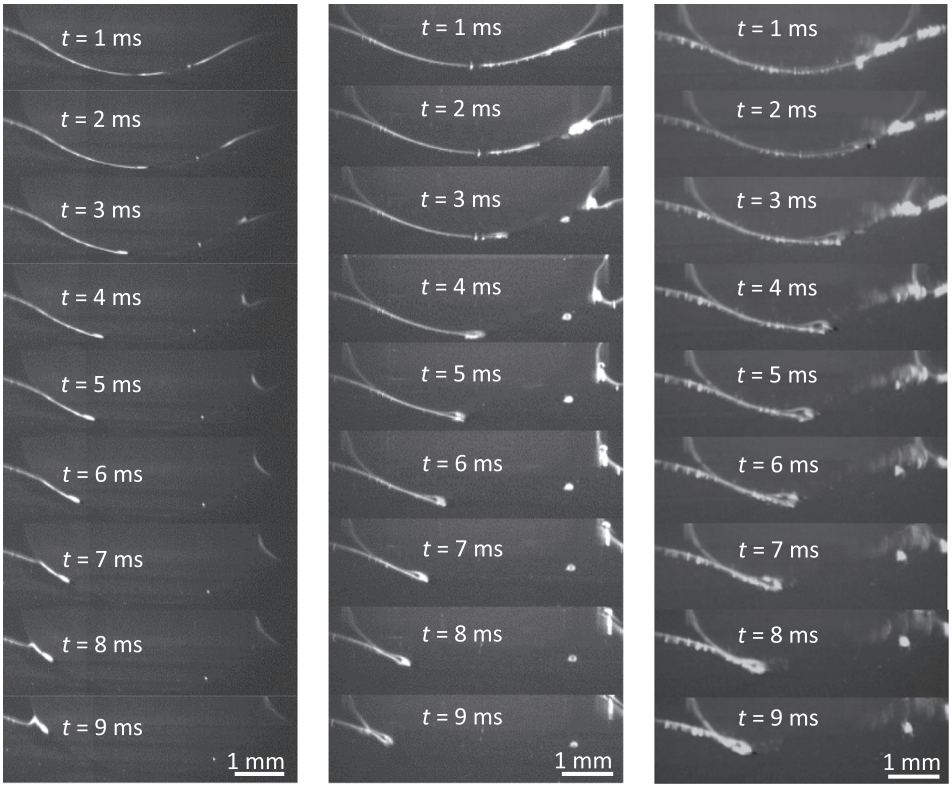

FIG. 9. Evolution of the local structure at the neck tip for different surface ages: (a) T = 0 min, (b) T = 240 min, and (c) T = 300 min.

the tip concentration can be seen as more surfactants are initially packed on the interface. For drop ages above 60 min, the increase in the tip concentration is not as high as would be expected and remains similar to that for T = 60 min. This is mainly attributed to a similar surfactant distribution along the interface for larger surface ages during the drop rest before the film rupture (see Fig. 7). In addition, as is shown in Fig. 12, the travel speeds of the tips for surface ages above 60 min

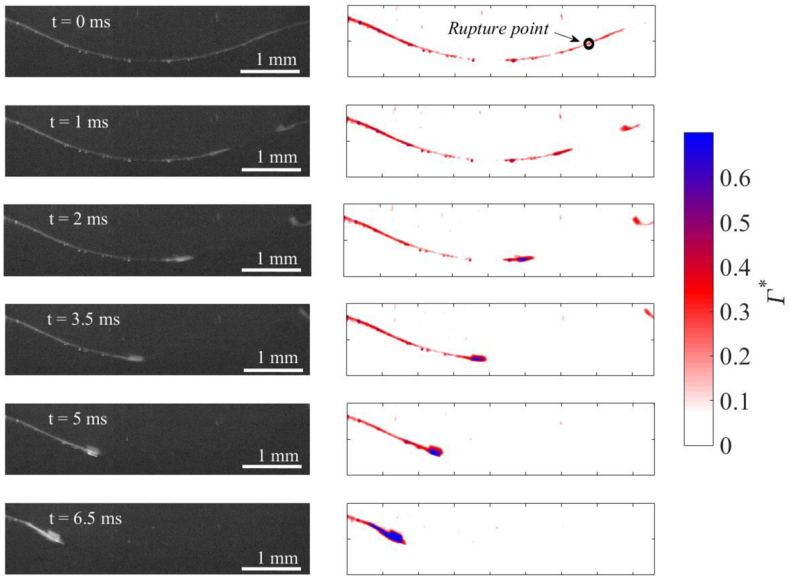

FIG. 10. The distribution of surfactant concentration Γ^* at the tip area during the neck growth for T = 0 min.

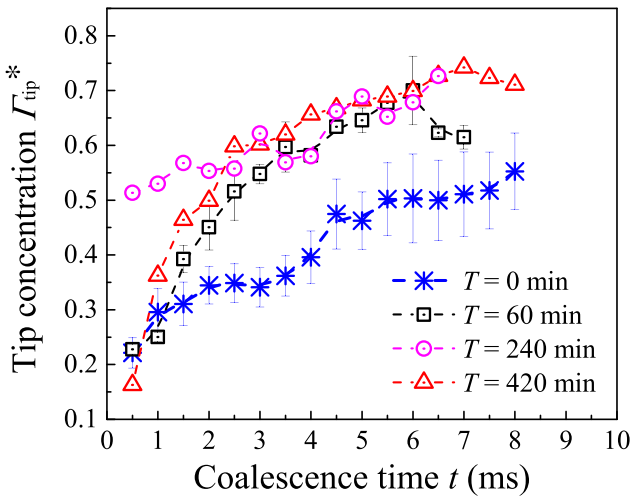

FIG. 11. Surfactant concentration at the tip of the neck for coalescences under different surface ages.

are close. As a result, the changes in the tip concentration for cases above 60 min do not vary a lot.

A different behaviour is observed for T = 240 min where the surfactant concentration becomes very high in the initial stages of the neck growth. This could be attributed to the initial uneven distribution of the surfactants along the interface before the rupture of the thin film. For T = 240 min, a large amount of surfactants is swept to the circumference to produce a high surfactant concentration on the right side, as shown in Fig. 7. When rupture occurs, a large amount of surfactant molecules has already been packed at the tip which gives the high tip concentration at the initial stages.

C. Distribution of surfactants along the drop surface

When surfactants are present, the reduction in the drop surface as it merges with the continuous bulk phase at the final stages of coalescence becomes slow and partial coalescence can be prevented.[37,39] This is attributed to the uneven distribution of surfactants on the drop surface.[32] The surfactant concentration along the coalescing surfaces is discussed in this section.

The concentration of surfactants along the surface of a coalescing drop for T = 720 min is shown in Fig. 13 as a representative example. The initial neck growth process was discussed in Sec. III B, and the results are shown here for the later stages of the drop merging with the bulk liquid. Previous studies have shown that a liquid cylinder forms in the later stages of coalescence.[38,64–66] From t = 20 ms to t = 36 ms, the top of the drop surface is stretched upwards by the convergence of the capillary waves initially formed after the meniscus rupture.[32,64,65,67] The surfactant concentration at the sides of the drop is higher compared to the top of the drop. The interface with the lower surfactant concentration on the top of the drop tends to pull the interface with the higher concentration at the bottom due to tangential Marangoni stresses.[33–36] On the other hand, the area at the phase interface away from the neck also has a low surfactant concentration and the resulting Marangoni stress drives the spreading of the surfactant along the phase interface away from the drop. At t = 39.5 ms when the liquid cylinder is created, the area with a high surfactant concentration is close to the summit of the drop. The distribution of surfactants agrees with the numerical findings by Martin and Blanchette.[32] Afterwards, the drop surface shrinks significantly until the liquid cylinder is about to pinch off at t = 45.5 ms. The average surfactant concentration in the drop increases because of the reduction in the area, especially at the top. As the Marangoni forces resist the convergence of the neck,[32,39] partial coalescence does not occur in this case.

To study the effect of surface age on the distribution of surfactants during the merging process, the surfactant concentration along the evolving surfaces was calculated at different T, as shown in Fig. 14. The figures on the right represent the corresponding evolution of the drop surface during coalescence. The profile of the drop surface is found by detecting

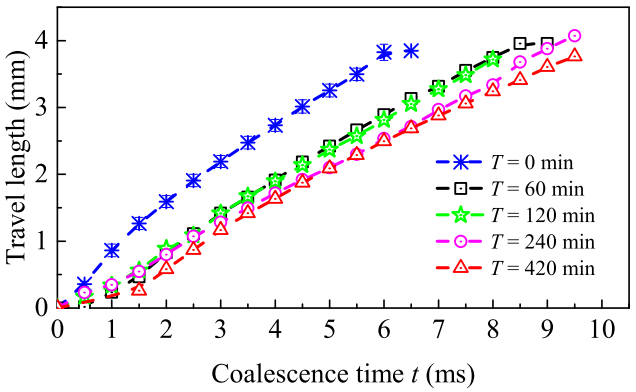

FIG. 12. Travel distance of the neck tip versus coalescence time for various drop surface ages. The travel length is defined as the distance of the tip away from its original location.

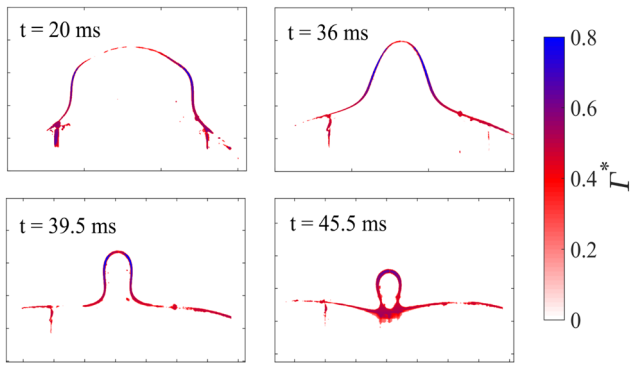

FIG. 13. Surfactant concentration Γ^* along the coalescing drop surface for T = 720 min.

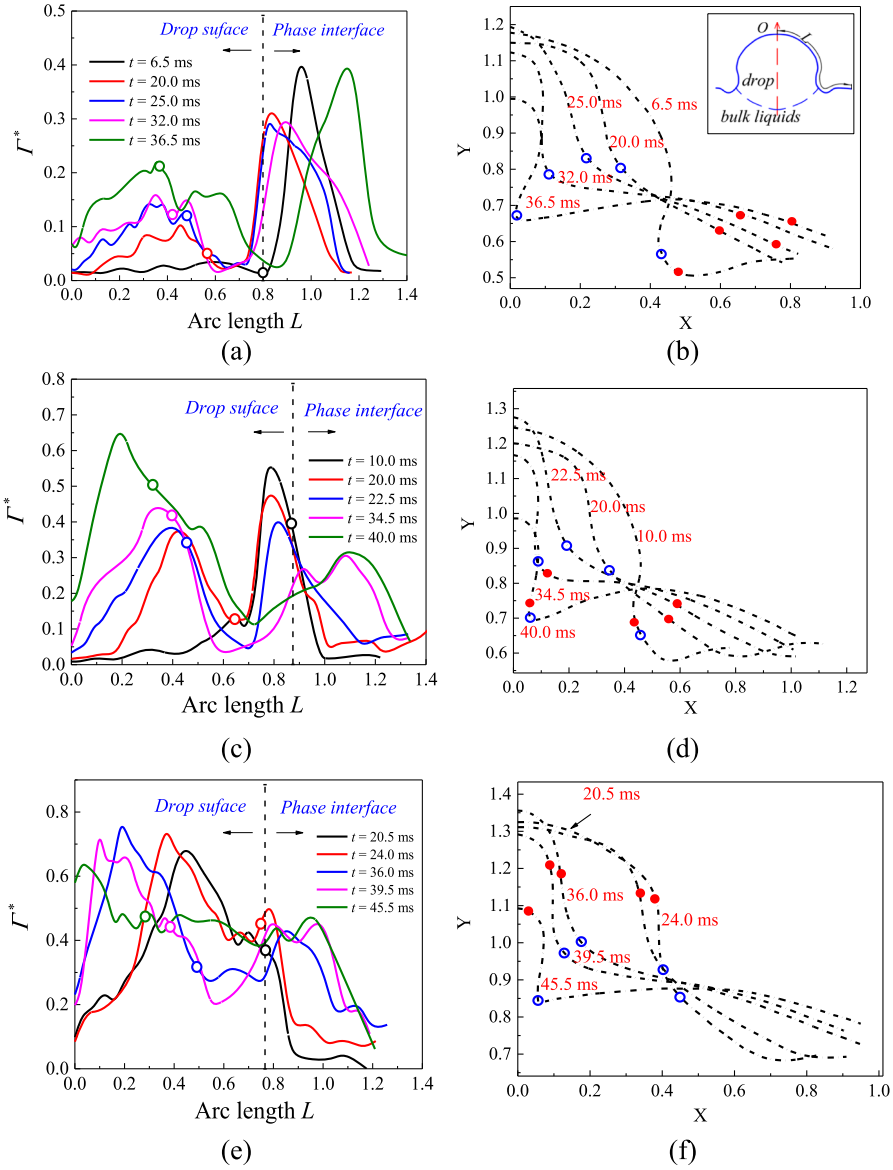

FIG. 14. Surfactant distributions along the deforming surfaces and the related evolution of the drop surface. The hollow circles in the figure indicate the positions of the neck edges, while the full (red) dots indicate the positions with the maximum surfactant concentration. (a) T = 0 min. (b) T = 0 min. (c) T = 60 min. (d) T = 60 min. (e) T = 720 min. (f) T = 720 min.

the boundary between the bright drop that has surfactant and the dark area in the surrounding liquid. As shown in the inset in Fig. 14(b), the surfactant concentration Γ^* along the arc was extracted following the method shown in Fig. 6. The arc length L, which was normalized by the horizontal diameter of the drop D_h, started at the drop summit O and terminated at the phase interface. The open points in the figure refer to the location of the neck edge. The locations with the highest surfactant concentration are denoted with the filled (red) points.

For T = 0 min, the peak of the surfactant concentration at t = 6.5 ms from the film rupture is observed at the bottom near the neck (corresponding arc length L = 0.95D_h), while the surfactant concentration is very low at the drop surface above the neck. This forms a boundary between the drop surface and the phase interphase, as plotted by the dashed line in Fig. 14(a). During the drop merging, the boundary may shift and not be so clear anymore; for this reason, only the boundary at the initial stage is plotted here to help visualization. From t = 20.0 ms to t = 32.0 ms, the drop surface is largely shrinking except from the top area which is being stretched by the capillary waves to create the liquid cylinder [Fig. 14(b)]. Over this process, the surfactant concentration at the drop sides above the neck is increased. After t = 32.0 ms, the top area of the drop stops expanding and starts to contract. Thus the surface concentration Γ^* at the top with L < 0.2D_h increases between t = 32.0 ms and t = 36.5 ms.

The peak value of Γ^* does not change too much at the bottom of the drop for $L > 0.7D_h$. At the early stages of coalescence, the peak concentration value slightly reduces from t = 6.5 ms to t = 25.0 ms but increases afterwards between t = 25.0 ms and t = 36.5 ms. This behaviour was shown as well by Martin and Blanchette[32] through simulation. The local variation of the surfactant concentration over the drop surface is controlled by two factors, the changes in the local surface area and the Marangoni forces along the drop surface. The Marangoni stresses tend to smooth out the uneven distribution of surfactant molecules along the interface, which is reflected in the decrease in the concentration peak from t = 6.5 ms to t = 25.0 ms. The contraction of the local surface area where the peak is located, on the other hand, may increase the concentration, which is seen from t = 25.0 ms to t = 36.5 ms. The concentration peak is located initially close to the neck edge (t = 6.5 ms) and then shifts away toward the phase interface, as shown in Fig. 14(b). As the global surfactant concentration gradually increases along the drop surface due to the surface contraction at $L < 0.7D_h$, the corresponding surface tension is lower than that of the phase interface on the right side of the peak. The resulting Marangoni stress between the peak and the drop surface is, therefore, weaker than that between the peak and the phase interface on the right side. In addition, the propagation of the waves that was initially created by the receding neck tends to shift the peak location outwards along the interface.[43,45] Therefore, the peak location gradually shifts away from the neck edge.

As the surface tension decreases when the drop surface is aged to T = 60 min, the evolution of the drop surface during coalescence is slower than at T = 0 min, as shown in Fig. 14(d). In addition, the increase in the surfactant concentration on the drop surface, resulting from the surface contraction, is significant. This large increase in the concentration decreases the Marangoni forces acting on the left side of the peak concentration (filled red dot) and increases the importance of the Marangoni forces between the peak location and the phase interface on the right. As a result, the concentration peak is slightly smoothened out forming plateaus towards the phase interface between t = 10.0 ms and t = 40.0 ms. Similar to T = 0 min, the location of the peak is on the phase interface and shifts away from the neck from t = 10.0 ms to t = 22.5 ms. However, from t = 34.5 ms, the concentration increases significantly at the drop and the peak is now found close to the neck again. At T = 720 min, the surfactant concentration on the drop surface is high. Thus, the increase in surfactant concentration caused by the drop contraction is larger at $L < 0.7D_h$ compared to both T = 0 min and T = 60 min. The peak location appears directly at the drop surface and on the left of the neck edge, in contrast to T = 0 min and T = 60 min where the concentration peaks appeared at the phase interface.

IV. CONCLUSIONS

In this paper, a high-speed PLIF technique is developed to investigate the surfactant concentration along the interfaces during the coalescence of aqueous drops with initially flat aqueous/organic interfaces. During the drop rest on the interface, the surfactants are found to accumulate at a barrier ring and increase locally the concentration in the film. These findings for the first time verify previous theoretical predictions.[20,22,54] The surfactant concentration at the ring increases as the interface age increases (higher initial surfactant concentration at the interfaces).

During the neck expansion after the rupture of the film, a bulge forms at the tip of the neck where the surfactant concentration is high compared to the rest of the area of the film. This confirms previous numerical findings and assumptions.[31,32] The surfactant concentration at the tip area is not constant but increases during the neck growth, which is more significant when the initial surfactant concentration at the interface is higher.

After the film has retracted, a peak in the surfactant concentration is observed at the meniscus at the bottom of the drop; the peak is smoothened by the action of Marangoni forces along the interface. In these final stages of coalescence, a liquid cylinder is formed as the drop surface is stretched upwards by capillary waves. The top of the cylinder has a low surfactant concentration. Gradually the concentration in the cylinder is increased as the cylinder shrinks from the combined action of the reduction in the interfacial area and upward Marangoni forces.

As the drop properties such as size, density, and the viscosity would change the coalescence regime[38,39] and influence the distribution of surfactants at the interfaces, future studies will investigate coalescence in different coalescence regimes.

ACKNOWLEDGMENTS

This work was funded by the UK Engineering and Physical Sciences Research Council (EPSRC) Programme Grant MEMPHIS. Teng Dong would like to thank the UCL-CSC Joint Scholarship for providing his studentship.

REFERENCES

[1] H. Farhadi, S. Riahi, S. Ayatollahi, and H. Ahmadi, "Experimental study of nanoparticle-surfactant-stabilized CO_2 foam: Stability and mobility control," Chem. Eng. Res. Des. **111**, 449–460 (2016).

[2] P. Venkataraman, J. Tang, E. Frenkel, G. L. McPherson, J. He, S. R. Raghavan, V. Kolesnichenko, A. Bose, and V. T. John, "Attachment of a hydrophobically modified biopolymer at the oilwater interface in the treatment of oil spills," ACS Appl. Mater. Interfaces **5**, 3572–3580 (2013).

[3] R. Han, A.-M. Zhang, S. Li, and Z. Zong, "Experimental and numerical study of the effects of a wall on the coalescence and collapse of bubble pairs," Phys. Fluids **30**, 042107 (2018).

[4] S. Tcholakova, N. D. Denkov, I. B. Ivanov, and B. Campbell, "Coalescence stability of emulsions containing globular milk proteins," Adv. Colloid Interface Sci. **123**, 259–293 (2006).

[5] L. Wang, Y. Gao, J. Li, M. Subirade, Y. Song, and L. Liang, "Effect of resveratrol or ascorbic acid on the stability of α-tocopherol in O/W emulsions stabilized by whey protein isolate: Simultaneous encapsulation of the vitamin and the protective antioxidant," Food Chem. **196**, 466–474 (2016).

[6]B. Andrade, Z. Song, J. Li, S. C. Zimmerman, J. Cheng, J. S. Moore, K. Harris, and J. S. Katz, "New frontiers for encapsulation in the chemical industry," ACS Appl. Mater. Interfaces **7**, 6359–6368 (2015).
[7]P. M. Somwanshi, K. Muralidhar, and S. Khandekar, "Coalescence dynamics of sessile and pendant liquid drops placed on a hydrophobic surface," Phys. Fluids **30**, 092103 (2018).
[8]B. W. Wagoner, S. S. Thete, and O. A. Basaran, "A new experimental method based on volume measurement for determining axial scaling during breakup of drops and liquid threads," Phys. Fluids **30**, 082102 (2018).
[9]E. Cockbain and T. McRoberts, "The stability of elementary emulsion drops and emulsions," J. Colloid Sci. **8**, 440–451 (1953).
[10]L. E. Nielsen, R. Wall, and G. Adams, "Coalescence of liquid drops at oil-water interfaces," J. Colloid Sci. **13**, 441–458 (1958).
[11]G. E. Charles and S. G. Mason, "The coalescence of liquid drops with flat liquid/liquid interfaces," J. Colloid Sci. **15**, 236–267 (1960).
[12]T. Hodgson and J. Lee, "The effect of surfactants on the coalescence of a drop at an interface. I ," J. Colloid Interface Sci. **30**, 94–108 (1969).
[13]T. Hodgson and D. Woods, "The effect of surfactants on the coalescence of a drop at an interface. II ," J. Colloid Interface Sci. **30**, 429–446 (1969).
[14]D. A. Edwards, H. Brenner, and D. T. Wasan, *Interfacial Transport Processes and Rheology* (Butterworth-Heinemann, 1991).
[15]D. T. Wasan, "Interfacial transport processes and rheology," Chem. Eng. Educ. **26**, 104 (1992).
[16]V. Cristini, J. Bawzdziewicz, and M. Loewenberg, "Near-contact motion of surfactant-covered spherical drops," J. Fluid Mech. **366**, 259–287 (1998).
[17]J. Bawzdziewicz, V. Cristini, and M. Loewenberg, "Near-contact motion of surfactant-covered spherical drops: Ionic surfactant," J. Colloid Interface Sci. **211**, 355–366 (1999).
[18]B. Dai and L. G. Leal, "The mechanism of surfactant effects on drop coalescence," Phys. Fluids **20**, 040802 (2008).
[19]L. Y. Yeo, O. K. Matar, E. S. P. de Ortiz, and G. F. Hewitt, "The dynamics of Marangoni-driven local film drainage between two drops," J. Colloid Interface Sci. **241**, 233–247 (2001).
[20]L. Y. Yeo, O. K. Matar, E. S. P. de Ortiz, and G. F. Hewitt, "Film drainage between two surfactant-coated drops colliding at constant approach velocity," J. Colloid Interface Sci. **257**, 93–107 (2003).
[21]E. Klaseboer, J. P. Chevaillier, C. Gourdon, and O. Masbernat, "Film drainage between colliding drops at constant approach velocity: Experiments and modeling," J. Colloid Interface Sci. **229**, 274–285 (2000).
[22]P. Ghosh and V. Juvekar, "Analysis of the drop rest phenomenon," Chem. Eng. Res. Des. **80**, 715–728 (2002).
[23]K. Giribabu and P. Ghosh, "Adsorption of nonionic surfactants at fluidfluid interfaces: Importance in the coalescence of bubbles and drops," Chem. Eng. Sci. **62**, 3057–3067 (2007).
[24]Z. Yan, I. C. Clark, and A. R. Abate, "Rapid encapsulation of cell and polymer solutions with bubble-triggered droplet generation," Macromol. Chem. Phys. **218**, 1600297 (2017).
[25]L.-H. Hung, K. M. Choi, W.-Y. Tseng, Y.-C. Tan, K. J. Shea, and A. P. Lee, "Alternating droplet generation and controlled dynamic droplet fusion in microfluidic device for CdS nanoparticle synthesis," Lab Chip **6**, 174–178 (2006).
[26]Q. Li and P. Angeli, "Experimental and numerical hydrodynamic studies of ionic liquid-aqueous plug flow in small channels," Chem. Eng. J. **328**, 717–736 (2017).
[27]J. Eggers, J. R. Lister, and H. A. Stone, "Coalescence of liquid drops," J. Fluid Mech. **401**, 293–310 (1999).
[28]D. G. Aarts and H. N. Lekkerkerker, "Droplet coalescence: Drainage, film rupture and neck growth in ultralow interfacial tension systems," J. Fluid Mech. **606**, 275–294 (2008).
[29]A. Eri and K. Okumura, "Bursting of a thin film in a confined geometry: Rimless and constant-velocity dewetting," Phys. Rev. E **82**, 030601 (2010).
[30]M. Yokota and K. Okumura, "Dimensional crossover in the coalescence dynamics of viscous drops confined in between two plates," Proc. Natl. Acad. Sci. U. S. A. **108**, 6395–6398 (2011).
[31]M. Chinaud, V. Voulgaropoulos, and P. Angeli, "Surfactant effects on the coalescence of a drop in a Hele-Shaw cell," Phys. Rev. E **94**, 033101 (2016).
[32]D. W. Martin and F. Blanchette, "Simulations of surfactant effects on the dynamics of coalescing drops and bubbles," Phys. Fluids **27**, 012103 (2015).
[33]E. Nowak, N. M. Kovalchuk, Z. Che, and M. J. Simmons, "Effect of surfactant concentration and viscosity of outer phase during the coalescence of a surfactant-laden drop with a surfactant-free drop," Colloids Surf., A **505**, 124–131 (2016).
[34]E. Nowak, Z. Xie, N. M. Kovalchuk, O. K. Matar, and M. J. Simmons, "Bulk advection and interfacial flows in the binary coalescence of surfactant-laden and surfactant-free drops," Soft Matter **13**, 4616 (2017).
[35]B. F. van Capelleveen, R. B. Koldeweij, D. Lohse, and C. W. Visser, "On the universality of Marangoni-driven spreading along liquid-liquid interfaces," preprint arXiv:1712.03192 (2017).
[36]F. Blanchette, L. Messio, and J. W. Bush, "The influence of surface tension gradients on drop coalescence," Phys. Fluids **21**, 072107 (2009).
[37]W. H. Weheliye, T. Dong, and P. Angeli, "On the effect of surfactants on drop coalescence at liquid/liquid interfaces," Chem. Eng. Sci. **161**, 215–227 (2017).
[38]X. Chen, S. Mandre, and J. J. Feng, "Partial coalescence between a drop and a liquid-liquid interface," Phys. Fluids **18**, 051705 (2006).
[39]T. Dong, W. H. Weheliye, P. Chausset, and P. Angeli, "An experimental study on the drop/interface partial coalescence with surfactants," Phys. Fluids **29**, 102101 (2017).
[40]F. Ravera, M. Ferrari, and L. Liggieri, "Adsorption and partitioning of surfactants in liquid–liquid systems," Adv. Colloid Interface Sci. **88**, 129–177 (2000).
[41]H. Jin, W. Wang, F. Liu, Z. Yu, H. Chang, K. Li, and J. Gong, "Roles of interfacial dynamics in the interaction behaviours between deformable oil droplets," Int. J. Multiphase Flow **94**, 44–52 (2017).
[42]S. Hosokawa, Y. Masukura, K. Hayashi, and A. Tomiyama, "Experimental evaluation of Marangoni stress and surfactant concentration at interface of contaminated single spherical drop using spatiotemporal filter velocimetry," Int. J. Multiphase Flow **97**, 157–167 (2017).
[43]D. W. Fallest, A. M. Lichtenberger, C. J. Fox, and K. E. Daniels, "Fluorescent visualization of a spreading surfactant," New J. Phys. **12**, 073029 (2010).
[44]S. L. Strickland, M. Shearer, and K. E. Daniels, "Spatiotemporal measurement of surfactant distribution on gravity–capillary waves," J. Fluid Mech. **777**, 523–543 (2015).
[45]E. R. Swanson, S. L. Strickland, M. Shearer, and K. E. Daniels, "Surfactant spreading on a thin liquid film: Reconciling models and experiments," J. Eng. Math. **94**, 63–79 (2015).
[46]S. L. Strickland, M. Hin, M. R. Sayanagi, C. Gaebler, K. E. Daniels, and R. Levy, "Self-healing dynamics of surfactant coatings on thin viscous films," Phys. Fluids **26**, 042109 (2014).
[47]J. Eastoe and J. Dalton, "Dynamic surface tension and adsorption mechanisms of surfactants at the air–water interface," Adv. Colloid Interface Sci. **85**, 103–144 (2000).
[48]J. Xu, Y. Zhang, H. Chen, P. Wang, Z. Xie, Y. Yao, Y. Yan, and J. Zhang, "Effect of surfactant headgroups on the oil/water interface: An interfacial tension measurement and simulation study," J. Mol. Struct. **1052**, 50–56 (2013).
[49]D. A. Edwards, H. Brenner, D. T. Wasan, and A. M. Kraynik, "Interfacial transport processes and rheology," Phys. Today **46**(4), 63 (1993).
[50]D. Langevin, "Bubble coalescence in pure liquids and in surfactant solutions," Curr. Opin. Colloid Interface Sci. **20**, 92–97 (2015).
[51]T. Morokuma and Y. Utaka, "Variation of the liquid film thickness distribution between contacting twin air bubbles during the coalescence process in water and ethanol pools," Int. J. Heat Mass Transfer **98**, 96–107 (2016).

[52]F. Yang, P. Tchoukov, P. Qiao, X. Ma, E. Pensini, T. Dabros, J. Czarnecki, and Z. Xu, "Studying demulsification mechanisms of water-in-crude oil emulsions using a modified thin liquid film technique," Colloids Surf., A **540**, 215 (2018).
[53]H. Princen, "Shape of a fluid drop at a liquid-liquid interface," J. Colloid Sci. **18**, 178–195 (1963).
[54]K. Burrill and D. Woods, "Film shapes for deformable drops at liquid-liquid interfaces. II. The mechanisms of film drainage," J. Colloid Interface Sci. **42**, 15–34 (1973).
[55]D. Y. Chan, E. Klaseboer, and R. Manica, "Film drainage and coalescence between deformable drops and bubbles," Soft Matter **7**, 2235–2264 (2011).
[56]G. Oldenziel, R. Delfos, and J. Westerweel, "Measurements of liquid film thickness for a droplet at a two-fluid interface," Phys. Fluids **24**, 022106 (2012).
[57]J.-D. Chen, P. S. Hahn, and J. Slattery, "Coalescence time for a small drop or bubble at a fluid-fluid interface," AIChE J. **30**, 622–630 (1984).
[58]J.-D. Chen and J. Slattery, "Effects of London-van der Waals forces on the thinning of a dimpled liquid film as a small drop or bubble approaches a horizontal solid plane," AIChE J. **28**, 955–963 (1982).
[59]J. L. Joye, G. J. Hirasaki, and C. A. Miller, "Dimple formation and behavior during axisymmetrical foam film drainage," Langmuir **8**, 3083–3092 (1992).
[60]D. A. Weiss and A. L. Yarin, "Single drop impact onto liquid films: Neck distortion, jetting, tiny bubble entrainment, and crown formation," J. Fluid Mech. **385**, 229–254 (1999).
[61]H. Aryafar and H. Kavehpour, "Hydrodynamic instabilities of viscous coalescing droplets," Phys. Rev. E **78**, 037302 (2008).
[62]H. P. Kavehpour, "Coalescence of drops," Annu. Rev. Fluid Mech. **47**, 245–268 (2015).
[63]L. Wang, G. Zhang, H. Wu, J. Yang, and Y. Zhu, "Note: A top-view optical approach for observing the coalescence of liquid drops," Rev. Sci. Instrum. **87**, 026103 (2016).
[64]F. Blanchette and T. P. Bigioni, "Partial coalescence of drops at liquid interfaces," Nat. Phys. **2**, 254–257 (2006).
[65]P. Yue, C. Zhou, and J. J. Feng, "A computational study of the coalescence between a drop and an interface in Newtonian and viscoelastic fluids," Phys. Fluids **18**, 102102 (2006).
[66]B. Ray, G. Biswas, and A. Sharma, "Generation of secondary droplets in coalescence of a drop at a liquid-liquid interface," J. Fluid Mech. **655**, 72–104 (2010).
[67]T. Gilet, K. Mulleners, J.-P. Lecomte, N. Vandewalle, and S. Dorbolo, "Critical parameters for the partial coalescence of a droplet," Phys. Rev. E **75**, 036303 (2007).